electronics

MDPI

Article

Joint Optimization of Trajectory and Discrete Reflection Coefficients for UAV-Aided Backscatter Communication System with NOMA

Chenyang Du [1], Jing Guo [1], Hanxiao Yu [1,*], Li Cui [2] and Zesong Fei [1]

[1] School of Information and Electronics, Beijing Institute of Technology (BIT), Beijing 100081, China; 3220225141@bit.edu.cn (C.D.); jingguo@bit.edu.cn (J.G.); feizesong@bit.edu.cn (Z.F.)
[2] College of Communications Engineering, Army Engineering University of PLA, Nanjing 210007, China
* Correspondence: yuhanxiao@bit.edu.cn

Abstract: Backscatter communication is a promising technology for the Internet of Things (IoT) systems with low-energy consumption, in which the data transmission of the backscatter devices relies on reflecting the incident signal. However, limited by the low power characteristic of the reflected signal from backscatter devices, achieving efficient data collection for the widely distributed backscatter devices is a thorny problem. Considering that unmanned aerial vehicles (UAVs) have flexible deployment capability, employing UAVs in a backscatter communication network can achieve feasible data collection for backscatter devices. In this paper, we consider a UAV-aided backscatter system and introduce Non-orthogonal multiple access (NOMA) to enable the UAV to collect signals from multiple backscatter devices simultaneously. We formulate an optimization problem to maximize the communication throughput of the considered system by jointly designing the backscatter device matching, the trajectory of the UAV, and the reflection coefficients of the backscatter devices, which is a non-convex optimization problem and challenging to solve. Hence, we decouple the original problem into three sub-problems and propose an efficient iterative algorithm based on Block Coordinate Descent (BCD) to solve them. In detail, a game-based matching algorithm is designed to ensure the transmission needs of remote backscatter devices. The UAV trajectory and reflection coefficients of backscatter devices are optimized through the Successive Convex Approximation (SCA) algorithm and relaxation algorithm. By iterative optimization of the sub-problems, the original problem is solved. The simulation results show that the proposed scheme can obtain a significant throughput gain compared to benchmark schemes.

Keywords: backscatter communication; UAV communication; NOMA; trajectory design; iterative algorithm

Citation: Du, C.; Guo, J.; Yu, H.; Cui, L.; Fei, Z. Joint Optimization of Trajectory and Discrete Reflection Coefficients for UAV-Aided Backscatter Communication System with NOMA. *Electronics* **2023**, *12*, 2029. https://doi.org/10.3390/electronics12092029

Academic Editor: Nurul I. Sarkar

Received: 28 March 2023
Revised: 23 April 2023
Accepted: 24 April 2023
Published: 27 April 2023

1. Introduction

1.1. State of the Art

The Internet of Things (IoT) is revolutionizing the world [1,2]. As self-sustainable devices without external power supply, backscatter devices (BDs) achieve signal transmission by reflecting incident signals, significantly facilitating the development of IoT networks towards low energy consumption and rapid deployment [3–6]. In [7], a mathematical framework of a backscatter communication (BackCom) model under an OFDM-based wireless communication system was proposed, and the theoretical analysis of capacity was developed. The authors of [8] considered a backscatter multiple access channel in which the receiver detected signals transmitted from both the carrier emitter (CE) and BD. Then, the achievable rate region and the detection error rate were analyzed. In [9], the authors proposed a spectrum sharing model to describe the backscattering communication system, and jointly optimized the transmit power of the CE and reflection coefficient of the BD to maximize the capacity of the BD reflecting link.

However, implementing the BackCom system faces serious challenges caused by the low power transmission capacity of the BDs, which results in the reachable communication ranges of BDs being small. Obviously, while deploying a large number of receivers could accomplish the required information collection, it would result in additional high deployment costs.

1.2. Related Work

In recent years, the application of unmanned aerial vehicles (UAVs) in communication has attracted more and more attention. For example, applying UAVs as sufficient tools to assist terrestrial networks has been eagerly discussed and intensively studied in [10–12], and the combination of intelligent reflecting surface with UAV technology is a promising communication technology that can be used to expand coverage and increase throughput [13,14]. Applying UAVs as the CE, relay, or receiver in the BackCom system has been recognized as an effective method to achieve highly efficient and fair data collection for the BackCom system [15–19]. In [17], a UAV was deployed as a CE to incentivize the BDs, and the BDs forwarded the signal to a ground receiver. Then, the time allocation, reflection coefficients, and UAV trajectory were jointly optimized to maximize the system capacity. The work in [18] proposed deploying a UAV as a flying BD to forward the signal from the source node to the receiver. Then, the total throughput was maximized by jointly optimizing the time allocation and the trajectory of the UAV. The authors of [19] treated the UAV as the receiver in the BackCom system and jointly optimized the UAV trajectory, BD scheduling, and transmitting power of the CEs to maximize energy efficiency. In particular, the UAVs acted as both the CEs and the receivers in [20], where the optimization problem was solved to ensure fairness between the BDs with the aim of maximizing the max-min rate of BDs.

On the other hand, with the rapid growth in the number of IoT devices, it is essential to support more devices with limited resources as well as to improve spectral efficiency. Therefore, power-domain non-orthogonal multiple access (NOMA) has been investigated for integration with the BackCom system [21–23]. A NOMA-enhanced BackCom System was considered in [24], and the BER performance of the considered system with imperfect successive interference cancellation (SIC) over an additive white Gaussian noise channel was derived. In [25,26], the authors investigated the communication scenarios where BDs coexisted with normal downlink users. The downlink signals sent from the base station to a user were reflected by multiple BDs simultaneously, then received and detected at the base station with the NOMA algorithm. The resource allocation schemes were then optimized to maximize the BD uplink throughput while considering the interference between the user downlink transmission and BD uplink transmission. In [27], the achievable sum rate of a NOMA-assisted ambient backscatter communication system was maximized by jointly optimizing the BD grouping, reflection coefficients, and decoding order.

1.3. Motivation and Contribution

In Table 1, we compare our work with existing works in terms of the optimization objective, UAV deployment, access scheme, and more. Unlike the existing works, we incorporate both NOMA and UAV communication into backscatter communication, with a UAV utilized to assist in the collection of signals transmitted simultaneously by multiple backscattering devices under the NOMA scheme. Moreover, considering that the communication link may be blocked during UAV communication, we consider a more realistic channel model, specifically, the probabilistic path loss channel model, which allows us to analyze the performance of the system more accurately. Furthermore, considering that the reflection coefficient of the BD is difficult to adjust continuously due to the hardware constraints present in actual deployment, we quantize the reflection coefficients of the BDs in the UAV-aided BackCom system into an achievable set $\mathcal{I}$. Facing the above-considered communication scenarios, jointly optimizing the BDs matching scheme, the trajectory of the UAV, and the reflection coefficients of the BDs is a challenging task, whereby the work

in this paper is innovative and has outstanding contributions. The main contributions of this paper are summarized below:

Table 1. Summary of our work and others in the literature.

Article	Objective	Apply UAV	Access Scheme	Number of BDs	BD Matching	Type of Reflection Coefficients
[17]	throughput	yes	TDMA	single	no	continuous variable
[18]	throughput	yes	TDMA	single	no	continuous variable
[19]	energy efficient	yes	TDMA	multiple	no	fixed constant 1
[20]	max-min rate	yes	TDMA	multiple	no	fixed constant 1
[24]	bit error rate	no	NOMA	double	no	continuous variable
[25]	throughput	no	NOMA	multiple	no	continuous values
[26]	throughput	no	NOMA	multiple	no	continuous values
[27]	throughput	no	NOMA	multiple	yes	continuous values
this article	throughput	yes	NOMA	multiple	yes	discrete set

(1) We investigate a UAV-aided BackCom network in which the BDs reflect the signals generated by the ground CEs and a flying UAV receives the data from the BDs with power-domain NOMA. We propose an optimization problem to maximize the communication throughput of the system and jointly optimize the BD matching scheme, trajectory of the UAV, and quantified reflection coefficients of the BDs.
(2) We formulate the optimization problem and transform the original non-convex problem into three sub-problems, namely, the BD matching problem, the trajectory optimization problem, and the reflection coefficient optimization problem, using the Block Coordinate Descent (BCD) algorithm [15,19,28–31]. Due to the sub-problems being non-convex, the game-based matching algorithm, the Successive Convex Approximation (SCA) algorithm, and the relaxation algorithm are applied to solve them iteratively.
(3) Finally, numerical results show that the scheme we propose achieves a significant improvement in communication throughput compared to the benchmark schemes, and has a fast convergence speed. It can be seen from the simulation results that the optimized trajectory of the UAV is more likely to concentrate above the BDs to maximize the communication throughput.

The rest of this paper is organized as follows. Section 2 introduces the system and formulates the communication throughput maximization problem for joint optimization of BD matching, UAV trajectory, and quantified reflection coefficients of BDs. In Section 3, the game-based matching algorithm and effective iterative algorithm are proposed to solve the optimization problem. In Section 4, numerical results are provided to verify the performance of the proposed scheme. Section 5 concludes the paper. The notation that appears in this paper is summarized in Table 2.

Table 2. Summary of Notation.

Notation	Description	Notation	Description
$\bar{K}$	the number of BDs associated with the same CE	$\mathcal{I}$	the predefined discrete reflection coefficient set
ϕ	the number of quantization levels of the backscatter coefficient	M	the number of CEs $(m \in 1, \ldots, M)$
K	the number of the BDs $(k \in 1, \ldots, K)$	T	the total communication period

Table 2. *Cont.*

Notation	Description	Notation	Description
$\mathbf{w}_k$	the coordinate of the k-th BD	$\mathbf{u}_m$	the coordinate of the m-th CE
$d_{m,k}$	the distance between the k-th BD and the m-th CE	N	the total number of slots ($n \in 1, \ldots, N$)
Δt	the duration of one slot	$\mathbf{q}(n)$	the coordinate of the UAV at the n-th slot
H	the height of the UAV	$d_{\mathrm{UB},k}(n)$	the distance between the k-th BD and the UAV at the n-th slot
$d_{\mathrm{UC},m}(n)$	the distance between the m-th CE and the UAV at the n-th slot	$PL_{m,k}$	the path loss between the m-th CE and the k-th BD
β_0	the channel power gain at the reference distance as 1 m	f	the communication frequency
c	the speed of light in vacuo	$PL_k^{\mathrm{LoS}}(n)$	the path loss of the Line-of-Sight channel
PL_k^{nLoS}	the path loss of the non-Line-of-Sight channel	κ_{LoS} & κ_{nLoS}	the attenuation factors of the Line-of-Sight and the non-Line-of-Sight channel
a & b	the air-to-ground channel parameter	$\theta_k(n)$	the angle of elevation between the UAV and the k-th BD at the n-th slot
$PR_k^{\mathrm{nLoS}}(n)$	the probability of Line-of-Sight channel	$PR_k^{\mathrm{nLoS}}(n)$	the probability of the non-Line-of-Sight channel
$PL_k^{\mathrm{avg}}(n)$	the average path loss between the UAV and the k-th BD at the n-th slot	$\boldsymbol{\alpha}(n)$	the active state of the BDs at the n-th slot ($\alpha_k(n) \in \boldsymbol{\alpha}(n)$)
$\gamma_k(n)$	the signal-to-interference-plus-noise ratio of the k-th BD at the n-th slot	$P_m(n)$	the transmitting power of the m-th CE at the n-th slot
σ^2	the power of the additive white Gaussian noise	$R(n)$	the throughput of the considered system at the n-th slot
B	the system bandwidth	$\boldsymbol{\eta}(n)$	the reflection coefficients of the BDs at the n-th slot ($\eta_k(n) \in \boldsymbol{\eta}(n)$)
$\check{R}$	the minimum throughput constraint threshold for a single BD	$\check{\gamma}$	the minimum signal-to-interference-plus-noise ratio constraint threshold
$\boldsymbol{q}_0$ & $\boldsymbol{q}_N$	the initial and termination coordinate of the UAV	$V_{\max}$	the maximum velocity of the UAV
ρ	the competition factor	I	the maximum number of iterations
ε	the convergence threshold	ΔR	the increment of the objective function
r	the number of iteration		

2. System Model and Problem Formulation

In this section, we introduce the considered UAV-aided BackCom system in detail, including the network architecture and the communication model.

2.1. Network Architecture

At any given moment, only one CE emits the signal, and $\bar{K}$ BDs associated with this CE are activated and reflect the signal while the other BDs remain inactive. The signals of multiple BDs are received at the UAV through the NOMA scheme and decoded by the SIC algorithm. The scheduling of BDs should be adjusted to ensure that the signals can be decoded successfully. In addition, considering that the continuous reflection coefficient is not suitable for implementation in engineering, we discretize the reflection coefficients of BDs selected from a predefined discrete reflection coefficient set $\mathcal{I}$. We set the discrete

reflection coefficient set $\mathcal{I}$ as uniformly sampled from the interval $[0,1]$, consisting of ϕ quantization levels.

As shown in Figure 1, we consider a UAV-aided BackCom system in which M CEs are deployed in a wide area to serve a group of K BDs. The sets of the CEs and BDs in this system are denoted as $\mathcal{M} = \{1,2,\ldots,M\}$ and $\mathcal{K} = \{1,2,\ldots,K\}$, respectively. First, one CE broadcasts the signal to activate the BDs, then the BDs modulate their data in keeping with the received signal and reflect it [19]. A UAV is deployed in this system to collect signals from the BDs on the ground in a continuous period $T > 0$.

We use a three-dimensional Cartesian coordinate system to describe the positions of the CEs, the BDs, and the trajectory of the UAV. The positions of the BDs and CEs can be expressed as $\mathbf{w}_k = [x_k, y_k, 0]^T \in R^{3\times 1}$, $1 \le k \le K$, and $\mathbf{u}_m = [x_m, y_m, 0]^T \in R^{3\times 1}$, $1 \le m \le M$. Then, the distance between the k-th BD and the m-th CE is represented by $d_{m,k} = \|\mathbf{w}_k - \mathbf{u}_m\|$, where the notation $||\cdot||$ denotes the 2 norm. To describe the trajectory of the UAV, the total communication period T is evenly divided into N slots [32]. Because a single slot $\Delta t = T/N$ is sufficiently small, the position of the UAV at one slot can be considered unchanged. Hence, the coordinate of the UAV at the n-th slot is represented as $\mathbf{q}(n) = [x_{UAV}(n), y_{UAV}(n), H]^T \in R^{3\times 1}$ for $n = 1,2,\ldots,N$, where H is the height of the UAV. Therefore, the distance between the k-th BD and the UAV at the n-th slot is provided by $d_{\mathrm{UB},k}(n) = \|\mathbf{w}_k - \mathbf{q}(n)\|$, while the distance between the m-th CE and the UAV at the n-th slot is represented by $d_{\mathrm{UC},m}(n) = \|\mathbf{u}_m - \mathbf{q}(n)\|$.

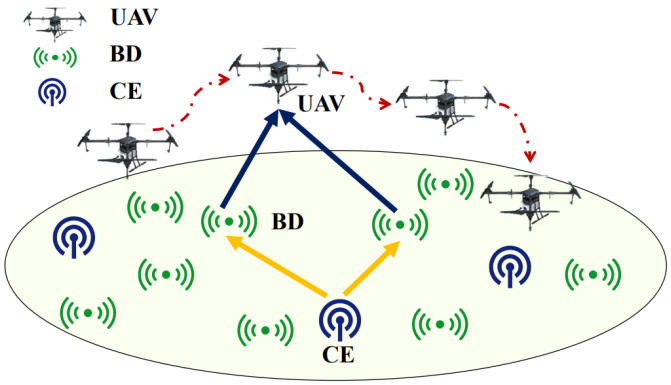

Figure 1. Description of the UAV-aided BackCom system.

2.2. Communication Model

Considering a more practical communication scenario, we assume that the links between the CE and BDs are Rayleigh channels with large-scale fading coefficients; only the spatial path loss is considered in this work. The path loss between the m-th CE and the k-th BD can be expressed as

$$PL_{m,k} = \frac{d_{m,k}^2}{\beta_0}, \tag{1}$$

where β_0 is the channel power gain at the reference distance of 1 m, which can be expressed as

$$\beta_0 = \frac{c^2}{(4\pi f)^2}, \tag{2}$$

where f and c are denoted as the communication frequency and the speed of light in vacuo, respectively. Considering that the link between the UAV and the k-th BD may be blocked

by obstacles, we consider the probabilistic path loss channel model [33]. The path loss of the Line-of-Sight (LoS) and non-Line-of-Sight (nLoS) channels can be expressed as

$$PL_k^{\mathrm{LoS}}(n) = \frac{d_{\mathrm{UB},k}^2}{\beta_0}\kappa_{\mathrm{LoS}}, \tag{3}$$

$$PL_k^{\mathrm{nLoS}} = \frac{d_{\mathrm{UB},k}^2}{\beta_0}\kappa_{\mathrm{nLoS}}, \tag{4}$$

where κ_{LoS} and κ_{nLoS} are additional attenuation factors of LoS and NLoS.

The LoS probability of the link from the k-th BD to the UAV can be expressed as

$$PR_k^{\mathrm{LoS}}(n) = \frac{1}{1 + a\exp(-b(\theta_k(n) - a))}, \tag{5}$$

where a and b are air-to-ground channel parameters which depend on the environment and $\theta_k(n)$ is the angle of elevation between the UAV and the k-th BD, which can be expressed as

$$\theta_k(n) = \frac{180}{\pi}\sin^{-1}\left(\frac{H}{d_{\mathrm{UB},k}(n)}\right). \tag{6}$$

The probability of nLoS is provided by $PR_k^{\mathrm{nLoS}}(n) = 1 - PR_k^{\mathrm{LoS}}(n)$. Then, the average path loss between the UAV and the k-th BD can be obtained as follows:

$$PL_k^{\mathrm{avg}}(n) = PR_k^{\mathrm{LoS}}(n)PL_k^{\mathrm{LoS}}(n) + PR_k^{\mathrm{nLoS}}(n)PL_k^{\mathrm{nLoS}}(n). \tag{7}$$

We define the binary variables $\boldsymbol{\alpha}(n) = \{\alpha_k(n), k = 1, 2, \ldots, K\}$ to indicate the active state of the BDs at the n-th slot, where $\alpha_k(n) = 1$ indicates that the k-th BD is activated and reflects the signal to the UAV at the n-th slot; otherwise, $\alpha_k(n) = 0$. Under the NOMA transmission scheme of the BDs, the decoding order at the UAV for BDs activated at the same slot is from the 1-th to the N-th BD, where we arrange the BDs in order of signal strength. Then, with the given channel model and the active indicators of the BDs, the signal-to-interference-plus-noise ratio (SINR) of the k-th BD at the n-th slot can be expressed as

$$\gamma_k(n) = \frac{\alpha_k(n)\eta_k(n)\frac{1}{PL_k^{\mathrm{avg}}(n)}\sum_{m=1}^{M} P_m(n)\frac{1}{PL_{m,k}}}{\sigma^2 + \sum_{j=k+1}^{K}\alpha_j(n)\eta_j(n)\frac{1}{PL_j^{\mathrm{avg}}(n)}\sum_{m=1}^{M} P_m(n)\frac{1}{PL_{m,j}}}, \tag{8}$$

where $P_m(n)$ is the transmitting power of the m-th CE at the n-th slot, $P_m(n) = 0$ indicates that the n-th CE is inactive, σ^2 represents the power of the additive white Gaussian noise, and $\eta_k(n)$ is the reflection coefficient of the k-th BD at the n-th slot. Then, the throughput of the considered system at the n-th slot is provided by

$$R(n) = \sum_{k=1}^{K}\Delta t\alpha_k(n)B\log_2(1 + \gamma_k(n)), \tag{9}$$

where B represents the system bandwidth.

2.3. Problem Formulation

In this section, we formulate the optimization problem to maximize the total throughput of the considered UAV-aided BackCom system in which the trajectory of the UAV

and deployment of the BDs are jointly optimized. We define $\boldsymbol{\eta}(n) \triangleq \{\eta_k(n), k = 1, \ldots, K\}$. Mathematically, the optimization problem can be expressed as

$$(\mathcal{P}_1) \quad \max_{\boldsymbol{\eta}(n),\mathbf{q}(n),\boldsymbol{\alpha}(n)} \sum_{n=1}^{N}\sum_{k=1}^{K} \Delta t \alpha_k(n) B \log_2(1+\gamma_k(n)) \tag{10a}$$

$$\text{s.t.} \quad \sum_{n=1}^{N} \Delta t \alpha_k(n) B \log_2(1+\gamma_k(n)) \geq \check{R}, \forall k, \tag{10b}$$

$$\gamma_k(n) \geq \check{\gamma}, \forall k, n, \tag{10c}$$

$$\sum_{k=1}^{K} \alpha_k(n) = \bar{K}, \forall n, \tag{10d}$$

$$\eta_k(n) \in \mathcal{I}, \forall k, n, \tag{10e}$$

$$\boldsymbol{q}(0) = \boldsymbol{q}_0, \boldsymbol{q}(N) = \boldsymbol{q}_N, \tag{10f}$$

$$\|\boldsymbol{q}(n+1) - \boldsymbol{q}(n)\| \leq V_{\max}\Delta t, \forall n, \tag{10g}$$

where (10b) ensures that the throughput of the k-th BD within the whole service time should be greater than the minimum rate $\check{R}$. To guarantee that each served BD can be decoded correctly at the UAV, the SINR of each BD is satisfied by the constraints (10c). Due to the limited capability of the UAV, we assume that a maximum of $\bar{K}$ BDs are allowed to access the UAV per slot, which is shown in (10d). In addition, considering that the circuit cannot generate continuously varying reflection coefficients, we assume that the reflection coefficients can be only selected from a quantified set $\mathcal{I}$, as the constraints (10e) indicate. Equation (10f) and inequality (10g) constrain the trajectory and velocity of the UAV, where $V_{\max}$ is the maximum velocity of the UAV. Due to the non-convex objective function and constraints in which the optimization variables are highly coupled with each other, the optimized problem is difficult to solve. The detailed algorithms for solving the non-convex problem are explained in detail in Section 3.

3. Proposed Solution

In this section, we propose a BCD-based algorithm to solve the formulated non-convex optimization problem. Specifically, to solve problem $\mathcal{P}_1$, we decouple the original problem into three sub-problems, i.e., the BD matching problem, the UAV trajectory optimization problem, and the reflection coefficient optimization problem, then respectively apply the game-based matching algorithm, SCA algorithm, and relaxation algorithm to solve these sub-problems. Afterwards, problem $\mathcal{P}_1$ can be solved by iteratively addressing the sub-problems until reaching convergence.

3.1. BD Matching Optimization

With the given fixed UAV trajectory and the reflection coefficients of the BDs, the BD matching problem is a nonlinear mixed-integer programming problem and is difficult to transform into a convex problem. Therefore, we propose a game-based matching algorithm to schedule the BDs effectively according to the locations of the CEs and BDs and the trajectory of the UAV. The game-based matching algorithm can be divided into four steps: (1) CE Scheduling; (2) BD Scheduling; (3) Slot Selection; and (4) Optional Set Updating.

(1) CE Scheduling

In this step, each slot is associated with a CE. Then, for each CE, an optional slot set is obtained by collecting its associated slots. For the n-th slot, we define the active CE as $\hat{m}_n$, which is obtained by

$$\hat{m}_n = \arg \min_{1 \leq m \leq M} (d_{\mathrm{UC},m}(n)). \tag{11}$$

We define the optional slot set for the m-th CE as $\mathcal{N}_m^{\mathrm{D}} \triangleq \{n \mid \hat{m}_n = m, \forall n\}$. Subsequently, we initialize the set of optional slots for the k-th BD as $\mathcal{N}_k^{\mathrm{B}} \triangleq \mathcal{N}_m^{\mathrm{D}}$, which indicates that the k-th BD is allocated slots to reflect the signal in the initialization of the proposed iterative algorithm.

(2) BD Scheduling

In this step, each BD selects one slot from its optional slot set based on transmission path loss. The selected slot for the k-th BD is expressed as

$$\hat{n}_k = \arg\min_{n \in \mathcal{N}_k^{\mathrm{B}}} (PL_{m,k} PL_k^{\mathrm{avg}}(n)). \tag{12}$$

We define the BDs that choose the n-th slot as the collected set $\mathcal{K}_n \triangleq \{k \mid \hat{n}_k = n, \forall k\}$. Note that more than one BD may choose the same slot. Hence, in the next step, an optimal BD is choesn for the n-th slot to reflect the signal from the set $\mathcal{K}_n$.

(3) Slot Selection

In this step, the slots selected by BDs in the previous step are used to select the most suitable BDs. For the n-th slot, the most suitable BD is selected from the set $\mathcal{K}_n$, which is defined as $\hat{k}_n$ and obtained by

$$\hat{k}_n = \arg\min_{k \in \mathcal{K}_n} (\frac{1}{N_k + \rho} PL_{m,k} PL_k^{\mathrm{avg}}(n)), \tag{13}$$

where N_k is the already-allocated number of slots for the k-th BD and ρ is the competition factor. Until this point, parts of BDs have been matched with the most appropriate slots; next, we update N_k with $N_k + 1$ if the k-th BD is chosen by one slot in this step. Otherwise, N_k remains unchanged.

(4) Optional Set Updating

After the previous two steps, we update the optional slot set belonging to each BD. When updating the optional slot set belonging to each BD, there are two principles to follow. First, the BDs and slots that already have a matching relationship cannot be matched again. Second, the number of BDs that can be matched per slot depends on $\bar{K}$. To update $\mathcal{N}_k^{\mathrm{B}}$, the slots are removed from the set $\mathcal{N}_k^{\mathrm{B}}$ if they satisfy any of the above principles.

Steps 2–4 are iterated until each slot matches $\bar{K}$ BDs, at which point the matching scheme $\boldsymbol{\alpha}(n)$ of each BD at slot n is obtained. The detailed game-based matching algorithm is shown in Algorithm 1. The matching scheme $\boldsymbol{\alpha}(n)$ is updated after Algorithm 1 if it increases the objective function (10a); otherwise, the previous $\boldsymbol{\alpha}(n)$ are utilized in solving the trajectory optimization problem and the reflection coefficient optimization problem.

Algorithm 1: Framework of the game-based matching algorithm.

Input: $\mathbf{w}_k$, $\mathbf{u}_m$, $\mathbf{q}(n)$ and ρ.
Output: The matching scheme $\boldsymbol{\alpha}(n)$ of BDs and slots.

1 Associate the CEs with the slots through (11).
2 **while** some slots do not match $\bar{K}$ BDs **do**
3 The BDs selects the target slot through (12).
4 Each slot select the best BD in $\mathcal{K}_n$ through (13). And increment the allocated number of slot belonging to this BD.
5 Update the optional slot set belonging to each BD.
6 **end**

3.2. Trajectory Optimization

With the fixed BD matching scheme and the reflection coefficients of the BDs, the trajectory optimization problem can be expressed as

$$(\mathcal{P}_2) \quad \max_{\mathbf{q}(n)} \sum_{n=1}^{N} \sum_{k=1}^{K} \Delta t \alpha_k(t) B \log_2(1 + \gamma_k(n)) \tag{14a}$$

$$s.t. \ \log_2(1 + \gamma_k(n)) \geq \log_2(1 + \check{\gamma}), \forall k, n, \tag{14b}$$

with the constraints (10b), (10f) and (10g). The constraint (14b) is equivalent to (10c).

Representing $\frac{1}{PL^k_{\text{avg}}(n)}$ as a variable $\Lambda_k(n)$, the objective function (14a) and left-hand side (LHS) of inequalities (14b) and (10b) are all non-convex with respect to $\Lambda_k(n)$. Because (14a) and the LHS of (14b) and (10b) have similar structures, we take (14a) as an example and transform it into a convex problem with respect to $\Lambda_k(n)$.

We first decompose the non-convex term in the logarithmic function of (14a), which is shown as

$$\begin{aligned}
&\log_2(1+\gamma_k(n)) \\
&= \log_2(1+\frac{\eta_k(n)\Lambda_k(n)\sum_{m=1}^{M} P_m(n)\frac{1}{PL_{m,k}}}{\sigma^2+\sum_{j=k+1}^{K}\alpha(n)\eta_j(n)\Lambda_j(n)\sum_{m=1}^{M} P_m(n)\frac{1}{PL_{m,j}}}) \\
&= \log_2(\sigma^2+\sum_{j=k}^{K}\alpha(n)\eta_j(n)\Lambda_j(n)\sum_{m=1}^{M} P_m(n)\frac{1}{PL_{m,j}}) \\
&\quad -\log_2(\sigma^2+\sum_{j=k+1}^{K}\alpha(n)\eta_j(n)\Lambda_j(n)\sum_{m=1}^{M} P_m(n)\frac{1}{PL_{m,j}}) \\
&= R_{1,k}(n)+R_{2,k}(n),
\end{aligned} \tag{15}$$

where

$$R_{1,k}(n) = \log_2(\sigma^2+\sum_{j=k}^{K}\alpha(n)\eta_j(n)\Lambda_j(n)\sum_{m=1}^{M} P_m(n)\frac{1}{PL_{m,j}}), \tag{16}$$

$$R_{2,k}(n) = -\log_2(\sigma^2+\sum_{j=k+1}^{K}\alpha(n)\eta_j(n)\Lambda_j(n)\sum_{m=1}^{M} P_m(n)\frac{1}{PL_{m,j}}). \tag{17}$$

Note that $R_{1,k}(n)$ and $R_{2,k}(n)$ are neither convex nor concave with respect to $\mathbf{q}(n)$. However, we find that $R_{1,k}(n)$ is a concave function with respect to $\Lambda_j(n)$ and that $R_{2,k}(n)$ is a convex function with respect to $\Lambda_j(n)$. Therefore, in the following we focus on obtaining the concave approximations of $R_{1,k}(n)$ and $R_{2,k}(n)$ with respect to $\mathbf{q}(n)$ based on $\Lambda_j(n)$.

For $R_{1,k}(n)$, we can obtain the linear lower bound of $R_{1,k}(n)$ using the SCA. For more detail, in the r-th iteration the first-order Taylor expansion is applied at the given local point $PL^r_{\text{avg},k}(n)$, then $R_{1,k}(n)$ is transformed into

$$\bar{R}_{1,k}(n) = \ln(\sigma^2+\sum_{j=k}^{K}\alpha(n)\eta_j(n)\bar{\Lambda}_j(n)\sum_{m=1}^{M} P_m(n)\frac{1}{PL_{m,j}})\log_2 e, \tag{18}$$

where e is the Euler constant and $\bar{\Lambda}_j(n)$ satisfies

$$\bar{\Lambda}_j(n) = \frac{2}{PL^r_{\text{avg},j}(n)} - \frac{1}{\left(PL^r_{\text{avg},j}(n)\right)^2}\tau_j(n), \forall j\in\{1,\ldots,K\}, \forall n, \tag{19}$$

where $\boldsymbol{\tau}(n) \triangleq \{\tau_j(n), j=1,\ldots,K\}$ are the slack variables and satisfy $\tau_j(n) \geq PL_{\text{avg},j}(n), \forall j \in \{1,\ldots,K\}, \forall n$. According to (3)–(7), we can now obtain

$$\tau_j(n) \geq \frac{d^2_{\text{UB},j}(n)}{\beta_0}(\kappa_{\text{nLoS}} + \frac{\kappa_{\text{nLoS}}-\kappa_{\text{nLoS}}}{1+a\exp(-b(\theta_j(n)-a))}), \forall j\in\{1,\ldots,K\}, \forall n. \tag{20}$$

Thus far, we have converted $R_{1,k}(n)$ into a concave form with respect to $\boldsymbol{\tau}(n)$. However, the new constraints (20) on $\boldsymbol{\tau}(n)$ remain non-convex. Next, we transform (20) into a convex form. For analytical convenience, we introduce new auxiliary variables $\boldsymbol{E}(n) \triangleq \{E_j(n), j=1,\ldots,K\}$, which satisfy

$$E_j(n) = \exp(-b(\theta_j(n)-a)), \forall j\in\{1,\ldots,K\}, \forall n, \tag{21}$$

and (20) can be expressed as

$$\ln \tau_j(n) \geq 2 \ln d_{\mathrm{UB},j}(n) - \ln \beta_0 + \ln(\kappa_{\mathrm{nLoS}} + \frac{\kappa_{\mathrm{LoS}} - \kappa_{\mathrm{nLoS}}}{1 + aE_j(n)}), \forall j \in \{1, \ldots, K\}, \forall n. \tag{22}$$

For the right half of the constraints in (22), $\ln d_{\mathrm{UB},j}(n)$ is concave with respect to $d_{\mathrm{UB},j}(n)$ and $\kappa_{\mathrm{nLoS}} + \frac{\kappa_{\mathrm{LoS}} - \kappa_{\mathrm{nLoS}}}{1+aE_j(n)}$ is concave with respect to $E_j(n)$, as κ_{LoS} is always equal to or greater than κ_{nLoS}. Next, we obtain the upper bound of $\ln d_{\mathrm{UB},j}(n)$ and $\ln(\kappa_{\mathrm{nLoS}} + \frac{\kappa_{\mathrm{LoS}} - \kappa_{\mathrm{nLoS}}}{1+aE_j(n)})$ in order to transform (22) into a convex expression.

First, we define $\boldsymbol{\zeta(n)} \triangleq \{\zeta_j(n), j = 1, \ldots, K\}$ as the upper bound of $\ln d_{\mathrm{UB},j}(n)$, $j = \{1, \ldots, K\}$ through first-order Taylor expansion at a local point $\mathbf{q}^r(n)$, which is provided by

$$\zeta_j(n) = \ln \left\| \mathbf{w}_j - \mathbf{q}^r(n) \right\| + \frac{1}{\left\| \mathbf{w}_j - \mathbf{q}^r(n) \right\|} \varrho_j(n) - 1, \forall j \in \{1, \ldots, K\}, \forall n, \tag{23}$$

where $\boldsymbol{\varrho(n)} \triangleq \{\varrho_j(n), j = 1, \ldots, K\}$ are the slack variables and satisfy

$$\varrho_j(n) \geq \left\| \mathbf{w}_j - \mathbf{q}(n) \right\|, \forall j \in \{1, \ldots, K\}, \forall n. \tag{24}$$

Then, we define $\boldsymbol{\mu(n)} \triangleq \{\mu_j(n), j = 1, \ldots, K\}$ as the upper bound of $\ln(\kappa_{\mathrm{nLoS}} + \frac{\kappa_{\mathrm{LoS}} - \kappa_{\mathrm{nLoS}}}{1+aE_j(n)}), \forall j \in \{1, \ldots, K\}, \forall n$, through first-order Taylor expansion at the given local point $E_j^r(n)$, which can be expressed as

$$\begin{aligned} \mu_j(n) = &\ln\left(\kappa_{\mathrm{nLoS}} + \frac{1}{1 + aE_j^r(n)}(\kappa_{\mathrm{LoS}} - \kappa_{\mathrm{nLoS}})\right) + \frac{a(\kappa_{\mathrm{nLoS}} - \kappa_{\mathrm{LoS}})(\bar{E}_j(n) - E_j^r(n))}{(\kappa_{\mathrm{nLoS}} aE_j^r(n) + \kappa_{\mathrm{LoS}})(aE_j^r(n) + 1)}, \\ &\forall j \in \{1, \ldots, K\}, \forall n, \end{aligned} \tag{25}$$

where $\bar{\boldsymbol{E}}(n) \triangleq \{\bar{E}_j(n), j = 1, \ldots, K\}$ are the slack variables and satisfy

$$\ln \bar{E}_j(n) \geq -b(\frac{180}{\pi} \sin^{-1}(\frac{H}{d_{\mathrm{UB},j}(n)}) - a), \forall j \in \{1, \ldots, K\}, \forall n. \tag{26}$$

With (23)–(26), we can transform (22) into

$$\ln \tau_j(n) \geq 2\zeta_j(n) - \ln \beta_0 + \mu_j(n), \forall j \in \{1, \ldots, K\}, \forall j \in \{1, \ldots, K\}, \forall n. \tag{27}$$

Until now, we have made the constraints (22) a convex expression. However, in the process of transforming (27), we have introduced the constraints (26), which are non-convex. For the in constraints (26), similar to the treatment of the inverse trigonometric function in [33], we have the upper bound of $-b(\frac{180}{\pi} \sin^{-1}(\frac{H}{d_{\mathrm{UB},j}(n)}) - a)$ through the first-order Taylor expansion at the local point $d_{\mathrm{UB},j}^r(n)$, and transform (26) into

$$\begin{aligned} \ln \bar{E}_j(n) \geq &-b(\frac{180}{\pi} \sin^{-1}(\frac{H}{d_{\mathrm{UB},j}^r(n)}) - a) + \frac{180b}{\pi} \frac{H(\iota_k(n) - d_{\mathrm{UB},j}^r(n))}{d_{\mathrm{UB},j}^r(n)\sqrt{d_{\mathrm{UB},j}^r(n) - H^2}}, \\ &\forall j \in \{1, \ldots, K\}, \forall n, \end{aligned} \tag{28}$$

where $\boldsymbol{\iota}(n) \triangleq \{\iota_j(n), j = 1, \ldots, K\}$ are the new slack variables and satisfy

$$\iota_j(n) \geq \left\| \mathbf{w}_j - \mathbf{q}(n) \right\|, \forall j \in \{1, \ldots, K\}, \forall n. \tag{29}$$

Thus far, we have obtained the concave approximation of $R_{1,k}(n)$. Next, we focus on $R_{2,k}(n)$.

$R_{2,k}(n)$ is a convex function about $\Lambda_j(n)$. However, we need find a concave form about $R_{2,k}(n)$ to solve $\mathcal{P}_2$. With the given local point $\Lambda_j^r(n)$ in the r-th iteration, we obtain the upper bound of $R_{2,k}(n)$ through the first-order Taylor expansion, which is provided by

$$\begin{aligned}\bar{R}_{2,k}(n) = &-(\ln(\sigma^2+\sum_{j=k+1}^{K}\alpha(n)\eta_j(n)\Lambda_j^r(n)\sum_{m=1}^{M}P_j(n)\frac{1}{PL_{m,j}})\\ &+\sum_{j=k+1}^{K}\frac{\alpha(n)\eta_j(n)(\chi_j(n)-\Lambda_j^r(n))\sum_{m=1}^{M}P_j(n)\frac{1}{PL_{m,j}}}{\sigma^2+\sum_{j=k+1}^{K}\alpha(n)\eta_j(n)\Lambda_j^r(n)\sum_{m=1}^{M}P_j(n)\frac{1}{PL_{m,j}}})\log_2 e,\end{aligned} \tag{30}$$

where $\boldsymbol{\chi}_j(n) \triangleq \{\chi_j(n), j=1,\ldots,K\}$ are auxiliary variables with the constraints $\chi_j(n) \geq \Lambda_j(n), \forall j \in \{1,\ldots,K\}$. Similar to (22), we use the logarithmic form to represent the constraints, which can be expressed as

$$\ln\chi_j(n) \geq \ln\beta_0 - \ln||\mathbf{w}_j-\mathbf{q}(n)||^2 - \ln(\kappa_{\mathrm{nLoS}}+\frac{\kappa_{\mathrm{LoS}}-\kappa_{\mathrm{nLoS}}}{1+aE_j(n)}), \forall j\in\{1,\ldots,K\}, \forall n. \tag{31}$$

Up to now, we have converted $R_{2,k}(n)$ to a convex form with respect to $\boldsymbol{\chi}(n)$. However, the new constraints (31) on $\boldsymbol{\chi}(n)$ are non-convex. Thus, we need to transform (31) into a convex form. In (31), we find that $||\mathbf{w}_j-\mathbf{q}(n)||^2$ is convex with respect to $\mathbf{q}(n)$ and $-\ln(\kappa_{\mathrm{nLoS}}+\frac{\kappa_{\mathrm{LoS}}-\kappa_{\mathrm{nLoS}}}{1+aE_j(n)})$ is convex with respect to $E_j(n)$. Then, we apply the first-order Taylor expansion to $||\mathbf{w}_j-\mathbf{q}(n)||^2$ based on the local point $\mathbf{q}^r(n)$ and introduce the new variables $\boldsymbol{\xi}(n) \triangleq \{\xi_j(n), j=1,\ldots,K\}$ to represent the lower bound of $\boldsymbol{E}(n)$. Finding that $E_j(n)$ is convex with respect to $\theta_j(n)$, we introduce the slack variables $\hat{\boldsymbol{\theta}}(n) \triangleq \{\hat{\theta}_j(n), j=1,\ldots,K\}$ and define $\xi_j(n)$ by applying the first-order Taylor expansion to $E_j(n)$ based on the local point $\theta_j^r(n)$, which can be obtained by

$$\xi_j(n) = \exp(-b(\theta_j^r(n)-a)) - b\exp(-b(\theta_j^r(n)-a))(\hat{\theta}_j(n)-\theta_j^r(n)), \forall j\in\{1,\ldots,K\}, \forall n, \tag{32}$$

with the constraints

$$\hat{\theta}_j(n) \geq \frac{180}{\pi}sin^{-1}(\frac{H}{||\mathbf{w}_j-\mathbf{q}(n)||}), \forall j\in\{1,\ldots,K\}, \forall n. \tag{33}$$

According to the above treatment, (31) can be transformed into

$$\begin{aligned}\ln\chi_j(n) \geq &\ln\beta_0 - \ln(||\mathbf{w}_j-\mathbf{q}^r(n)||^2+2(\mathbf{q}^r(n)-\mathbf{w}_j)(\mathbf{q}(n)-\mathbf{q}^r(n)))\\ &-\ln(\kappa_{\mathrm{nLoS}}+\frac{\kappa_{\mathrm{LoS}}-\kappa_{\mathrm{nLoS}}}{1+a\xi_j(n)}), \forall j\in\{1,\ldots,K\}, \forall n,\end{aligned} \tag{34}$$

which are convex with respect to $\mathbf{q}(n)$ and $\hat{\boldsymbol{\theta}}(n)$. Now, we have changed $R_{2,k}(n)$ into a concave form, and the constraints on the slack variables we added in the process of transformation are convex as well. After the above process, problem $\mathcal{P}_2$ can be expressed in the following form:

$$(\mathcal{P}_{2.1}) \quad \max_{\mathbf{q}(n),\boldsymbol{\tau}(n),\boldsymbol{\varrho}(n),\bar{\mathbf{E}}(n),\boldsymbol{\iota}(n),\boldsymbol{\chi}(n),\hat{\boldsymbol{\theta}}(n)} \sum_{n=1}^{N}\sum_{k=1}^{K}\Delta t\alpha_k(n)B(\bar{R}_{1,k}(n)+\bar{R}_{2,k}(n)) \tag{35a}$$

$$s.t. \quad \sum_{n=1}^{N}\Delta t\alpha_k(n)B(\bar{R}_{1,k}(n)+\bar{R}_{2,k}(n)) \geq \check{R}, \forall k, \tag{35b}$$

$$\bar{R}_{1,k}(n)+\bar{R}_{2,k}(n) \geq \log_2(1+\check{\gamma}), \forall k,n, \tag{35c}$$

with the constraints (10f), (10g), (24), (27)–(29), (33) and (34).

Note that problem $\mathcal{P}_{2.1}$ is a convex optimization problem, which can be solved by standard convex optimization solvers such as CVX.

3.3. Reflection Coefficient Optimization

With the given trajectory of the UAV and BD matching scheme, the optimization problem for the reflection coefficients of the BDs without the discrete constraint is provided by

$$(\mathcal{P}_3) \quad \max_{\boldsymbol{\eta}(n)} \sum_{n=1}^{N} \sum_{k=1}^{K} \Delta t \alpha_k(n) B \log_2(1+\gamma_k(n)) \tag{36a}$$

$$s.t. \quad 0 \le \eta_k(n) \le 1, \forall k, n, \tag{36b}$$

with the constraints (10b) and (14b).

It can be noted that the objective function in (36a) and the constraints (10b) and (14b) are non-convex for $\eta_k(n)$. Similar to the processing of (15), $\log_2(1+\gamma_k(n))$ in (36a) can be expressed as the sum of two terms, i.e., $R_{1,k}(n)$ and $R_{2,k}(n)$. It is clear that $R_{1,k}(n)$ is a concave function about $\eta_k(n)$, while $R_{2,k}(n)$ is a convex function about $\eta_k(n)$. Thus, our goal is to transform $R_{2,k}(n)$ into a concave form with respect to $\eta_k(n)$. Here, we use the first-order Taylor expansion to deal with $R_{2,k}(n)$ at the given local point $\eta_k^r(n)$ at the r-th iteration and introduce the new variables $\bar{\boldsymbol{\eta}}(n) \triangleq \{\bar{\eta}_k(n), k = 1, \ldots, K\}$; then, we can obtain the lower bound of $R_{2k}(n)$ as

$$\begin{aligned} \check{R}_{2,k}(n) = &- \lg(\sigma^2 + \sum_{j=k+1}^{K} \alpha(n)\eta_j^r(n) \frac{1}{PL_{\text{avg}}^j(n)} \sum_{m=1}^{M} P_m(n) \frac{1}{PL_{m,j}}) \\ &- \frac{\sum_{j=k+1}^{K} \alpha(n)(\bar{\eta}_j(n) - \eta_j^r(n)) \frac{1}{PL_{\text{avg}}^j(n)} \sum_{m=1}^{M} P_m(n) \frac{1}{PL_{m,j}}}{\sigma^2 + \sum_{j=k+1}^{K} \alpha(n)\eta_j^r(n) \frac{1}{PL_{\text{avg}}^j(n)} \sum_{m=1}^{M} P_m(n) \frac{1}{PL_{m,j}}}. \end{aligned} \tag{37}$$

Therefore, we can reformulate problem $\mathcal{P}_3$ as

$$(\mathcal{P}_{3.1}) \quad \max_{\bar{\boldsymbol{\eta}}(n)} \sum_{n=1}^{N} \sum_{k=1}^{K} \Delta t \alpha_k(n) B(R_{1,k}(n) + \check{R}_{2,k}(n)) \tag{38a}$$

$$s.t. \ \sum_{n=1}^{N} \Delta t \alpha_k(n) B(R_{1,k}(N) + \check{R}_{2,k}(n)) \ge \check{R}, \forall k, \tag{38b}$$

$$R_{1,k}(n) + \check{R}_{2,k}(n) \ge \log_2(1+\check{\gamma}), \forall k, n, \tag{38c}$$

$$0 \le \bar{\eta}_k(n) \le 1, \forall k, n. \tag{38d}$$

It can be noticed that problem $\mathcal{P}_{3.1}$ is a convex problem and can be solved directly. After continuous optimization of the backscattering coefficients, the discrete coefficients are obtained using downward rounding based on the discrete set $\mathcal{I} = \{0, \frac{1}{I}, \frac{2}{I}, \ldots, 1\}$, where $I = \phi - 1$, which can be expressed as

$$\eta_k(n) = \begin{cases} \frac{i}{I}, & \text{if } \frac{i}{I} \le \bar{\eta}_k(n) < \frac{i+1}{I}, \ i = 0, \ldots, I-1 \\ 1, & \text{if } \bar{\eta}_k(n) = 1. \end{cases} \tag{39}$$

3.4. Overall Algorithm

Based on the solutions to the sub-problems, the original problem $\mathcal{P}_1$ can be efficiently solved through the BCD-based iterative optimization algorithm, which is shown in Algorithm 2. When we update one of the variables, the other two variables are fixed and the corresponding solution is conducted to obtain an optimal result under this situation. Then, the three variables are updated iteratively. We show a flowchart of Algorithm 2 in Figure 2 to illustrate the detailed steps of each solution more clearly.

Algorithm 2: BCD-Based Algorithm for solving problem $\mathcal{P}_1$.

Input: Convergence threshold ε, the maximum number of iterations F.
Output: $\boldsymbol{\eta}(n)$, $\mathbf{q}(n)$, $\boldsymbol{\alpha}(n)$.

Initialize the variables $\boldsymbol{\eta}^0(n)$, $\mathbf{q}^0(n)$. Let $r = 1$.
while the increment of the objective function ΔR is greater than the threshold ε or the maximum number of iterations F has no been reached **do**
    The matching scheme of BDs and slots $\boldsymbol{\alpha}(n)$ are obtained by **Algorithm 1**.
    Solve the problem $\mathcal{P}_{2.1}$, and obtain the trajectory of the UAV $\mathbf{q}^r(n)$.
    Solve the problem $\mathcal{P}_{3.1}$, and obtain the reflection coefficients $\boldsymbol{\eta}^r(n)$.
    Obtain the discrete reflection coefficients through (39).
    Update $r = r + 1$.
end

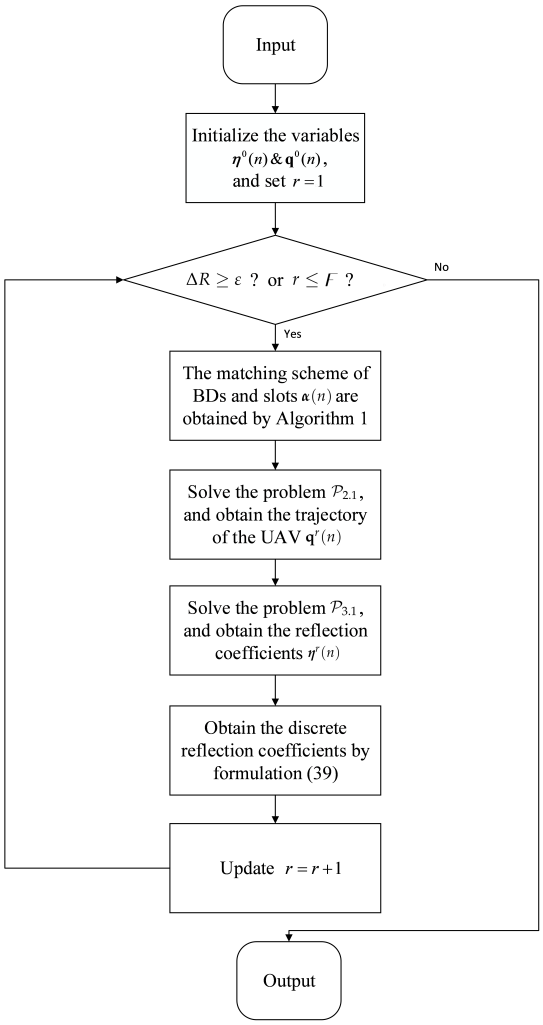

Figure 2. Flowchart of Algorithm 2.

3.4.1. Algorithm Convergence Analysis

In this subsection, the convergence of the optimization algorithm is analyzed. We denote the whole throughput of the UAV-aided BackCom system at the r-th iteration as $CV(\boldsymbol{\alpha}^r(n), \boldsymbol{q}^r(n), \boldsymbol{\eta}^r(n))$.

In Algorithm 2, it follows that

$$\begin{aligned} & CV(\boldsymbol{\alpha}^r(n), \boldsymbol{q}^r(n), \boldsymbol{\eta}^r(n)) \\ & \overset{(a)}{\leq} CV(\boldsymbol{\alpha}^{r+1}(n), \boldsymbol{q}^r(n), \boldsymbol{\eta}^r(n)) \\ & \overset{(b)}{\leq} CV_{bl}(\boldsymbol{\alpha}^{r+1}(n), \boldsymbol{q}^{r+1}(n), \boldsymbol{\eta}^r(n)) \\ & \overset{(c)}{=} CV(\boldsymbol{\alpha}^{r+1}(n), \boldsymbol{q}^{r+1}(n), \boldsymbol{\eta}^r(n)) \\ & \overset{(d)}{\leq} CV_{bl}(\boldsymbol{\alpha}^{r+1}(n), \boldsymbol{q}^{r+1}(n), \boldsymbol{\eta}^{r+1}(n)) \\ & \overset{(e)}{=} CV(\boldsymbol{\alpha}^{r+1}(n), \boldsymbol{q}^{r+1}(n), \boldsymbol{\eta}^{r+1}(n)), \end{aligned} \tag{40}$$

where the inequality (*a*) holds because Algorithm 1 is applied by fixing trajectory $\boldsymbol{q}^r(n)$ and reflection coefficient $\boldsymbol{\eta}^r(n)$. Inequality (*b*) comes from the fact that the trajectory $\boldsymbol{q}^{r+1}(n)$ is optimized by fixing the reflection coefficient $\boldsymbol{\eta}^r(n)$ and matching scheme $\boldsymbol{\alpha}^{r+1}(n)$ in the trajectory optimization part. Equality (*c*) holds because problem $\mathcal{P}_{2.1}$ we have optimized is the tight lower bound of $\mathcal{P}_2$. Inequality (*d*) proves that the whole throughput is improved after optimizing the reflection coefficient by fixing the trajectory $\boldsymbol{q}^{r+1}(n)$ and matching scheme $\boldsymbol{\alpha}^{r+1}(n)$. Finally, inequality (*e*) proves that problem $\mathcal{P}_{3.1}$ we have optimized is the tight lower bound of the original sub-problem $\mathcal{P}_3$. It can be seen from the above that the continuous iteration of the sub-problems shows an increasing trend of the objective function. Becuase there is an upper limit on the total amount of traffic due to fixed time and bandwidth resources, the proposed Algorithm 2 is guaranteed to converge.

3.4.2. Complexity Analysis

In Algorithm 1, the complexity of CE scheduling, BD selection, slot selection, and optional set updating can be expressed as $O_1(NM)$, $O_2(NK)$, $O_3(NK)$, and $O_4(K)$ for the worst-case scenario [34].

In Algorithm 2, we pay attention to the sub-problems whose complexity comes from solving the convex optimization problem. In trajectory optimization, the original non-convex problem is transformed into $\mathcal{P}_{2.1}$ using the SCA method. Denoting the number of variables as $N_1 = (6K+2)N$ and the number of constraints as $C_1 = 7NK + K + N + 2$, the complexity of $\mathcal{P}_{2.1}$ is $O_5((N_1 + C_1)^{3/2} N_1^2)$ [35]. For the reflection coefficient optimization, denoting the number of variables as $N_2 = KN$ and the number of constraints as $C_2 = 2NK + K$, the complexity of $\mathcal{P}_{3.1}$ is $O_6((N_2 + C_2)^{3/2} N_2^2)$.

By assuming that the number of iterations of Algorithm 2 is I_s, the complexity of Algorithm 2 is $O(I_s(NK + (N_1 + C_1)^{3/2} N_1^2 + (N_2 + C_2)^{3/2} N_2^2))$.

4. Simulation Results

In this section, we demonstrate the effectiveness of the proposed algorithm under different simulation conditions. As a comparison, we use three benchmark schemes: (1) an optimized scheme using the time-division multiple access (TDMA) method; (2) an optimized scheme based on the continuous reflection coefficient; and (3) a pre-optimization scheme that uses a circular trajectory for the UAV. We consider a system in which there are two CEs $M = 2$, each of which is responsible for an area of 50 square meters. There are $K = 12, 16, \ldots, 32$ BDs randomly distributed in the system. We set the period of the system communication and the height of the UAV as $T = 45, 47, 49, \ldots, 65$ s and $H = 18, 20, 22, \ldots, 30$ m, respectively. Unless specifically clarified, the applied simulation parameters in this paper are as shown in Table 3.

Table 3. Simulation parameters.

Parameter	Description	Value
B	the system bandwidth (MHz)	1
f	the communication frequency (MHz)	900
$V_{\max}$	the maximum velocity of the UAV (m/s)	10 [19]
σ^2	the power of the additive white Gaussian noise (dBm)	−140 [19,32]
P_m	the transmitting power of the m-th CE (W)	3
N	the total number of slots	50
H	the height of the UAV (m)	20
K	the number of the BDs	16
T	the total communication period(s)	50
$\check{R}$	the minimum throughput constraint threshold for a single BD (Mbit)	10
$\check{\gamma}$	the minimum signal-to-interference-plus-noise ratio constraint threshold (dB)	0
ϕ	the number of quantization levels of the backscatter coefficient	8
ρ	the competition factor	1
a	the air-to-ground channel parameter	9.6 [33]
b	the air-to-ground channel parameter	0.28 [33]
κ_{LoS}	the attenuation factor of the LoS channel (dB)	1 [33]
κ_{nLoS}	the attenuation factor of the nLoS channel (dB)	20 [33]

In Figure 3, we compare the total communication throughout under different numbers of BDs with $T = 50$ s and $H = 20$ m. From Figure 3, we can observe that the proposed scheme with NOMA achieves a much higher throughput under different BDs numbers than that based on TDMA, and closely approximates the scheme with continuous reflection coefficients. In the scenario with 32 BDs, the optimized scheme achieves a 14.7% throughput gain relative to the pre-optimization scheme.

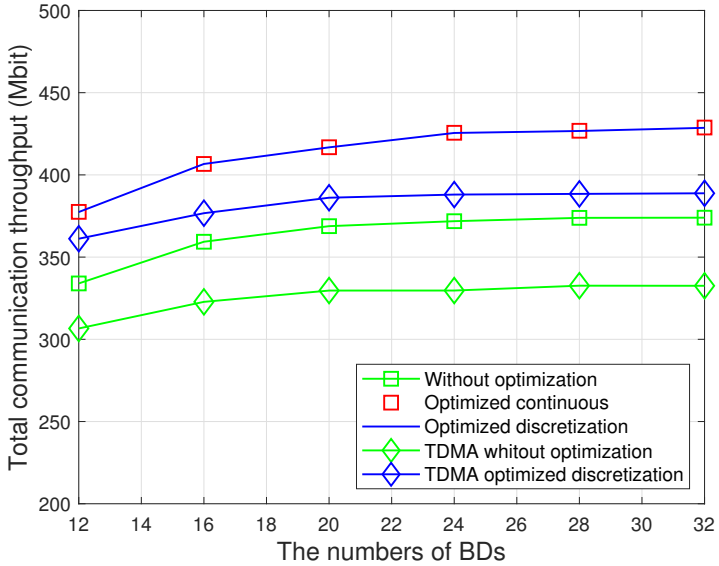

Figure 3. Total communication throughput with different numbers of BDs.

In Figure 4, we illustrate the initial UAV trajectory and the optimized UAV trajectory under $K = 16$, $T = 50$ s, $H = 20$ m. After optimization, the UAV flies close to the BDs to reduce the spatial loss and improve the throughput. Meanwhile, due to the NOMA strategy, the setting of the start and stop positions, and the constraints on the UAV's flight speed, the UAV does not need to fly directly over each BD to receive the signals.

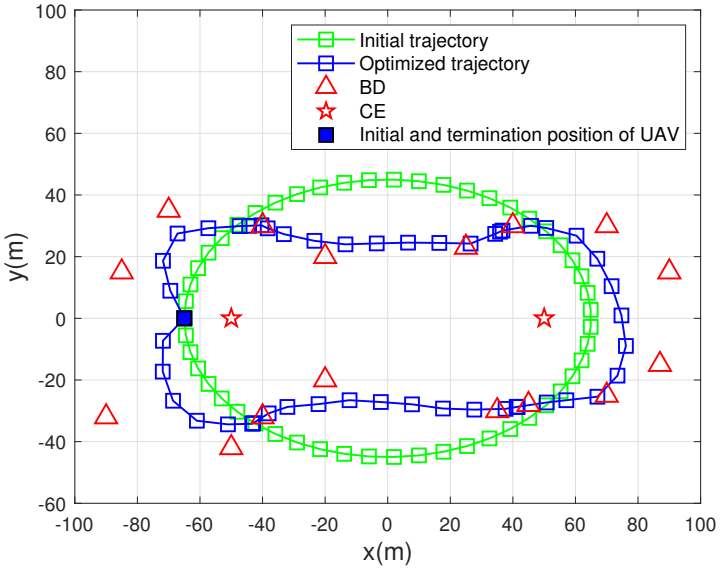

Figure 4. Optimized trajectory.

We illustrate the convergence of Algorithm 2 with different numbers of BDs in Figure 5 under $T = 50$ s, $H = 20$ m. With different numbers of BDs, the total system throughput optimized by Algorithm 2 is quickly completed within six iterations, verifying the fast convergence of the algorithm.

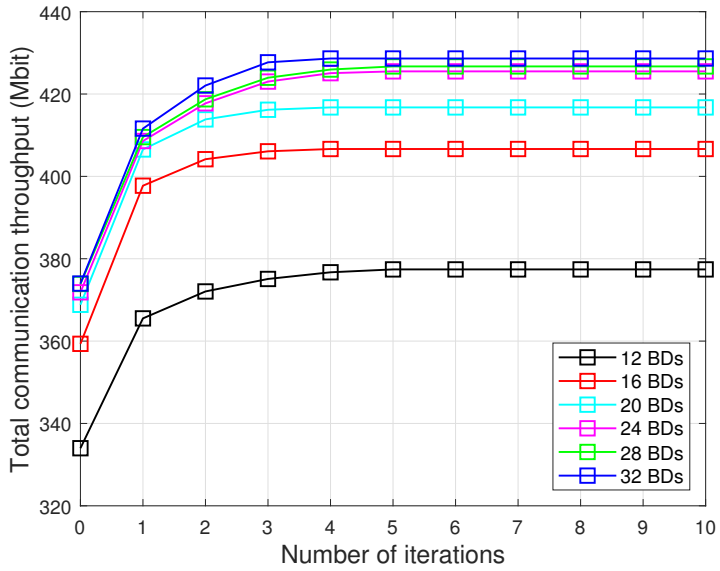

Figure 5. Convergence of Algorithm 2.

By setting the number of BDs $K = 16$ and the height of UAV $H = 20$ m, we illustrate the frequency band utilization under different system communication periods in Figure 6. As a result, it can be observed that the average throughput optimized by Algorithm 2 is better than the benchmark schemes using the TDMA method and circle trajectory of the UAV under any communication period.

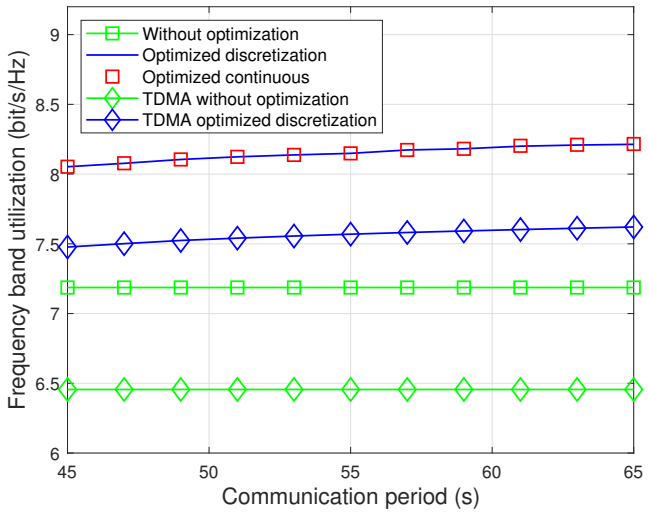

Figure 6. Frequency band utilization of different communication periods.

In Figure 7, we illustrate the impact of the flying height of the UAV in the considered system under $K = 16$, $T = 50$ s. It can be seen from Figure 7 that the total communication throughput is significantly improved at different heights after optimization. From Figure 7, it can be observed that in the scheme without the proposed optimization the throughput deteriorates more significantly with a height of around 20 m. However, through the optimization method proposed in this paper, the performance deterioration due to NLoS with the UAV height around 20 m is mitigated. Therefore, the proposed scheme can achieve a more significant performance gain at 20 m height, as shown in Figure 7.

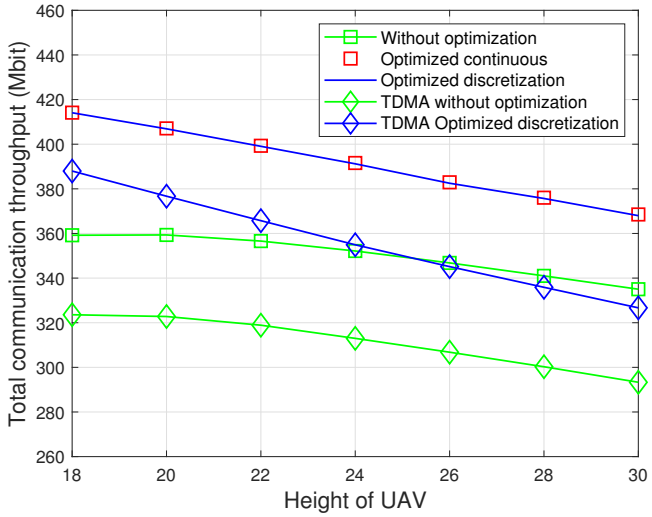

Figure 7. Total communication throughput of different UAV heights.

5. Conclusions

This paper investigated a UAV-aided BackCom system using the power domain NOMA scheme, along with formulation of a throughput maximization problem. Due to the high coupling between optimization variables in the original problem, we have proposed a BCD-based algorithm to jointly optimize the BD matching, UAV trajectory, and discrete reflection coefficients. Our simulation results demonstrate that the proposed algorithm can greatly improve the throughput of the system compared with benchmark schemes, and that it exhibits fast convergence. In our future work, we intend to investigate more practical scenarios incorporating BDs that coexist with normal ground users, multiple UAVs

jointly being deployed for data collection, and an intelligent reflecting surface-assisted UAV communication system.

Author Contributions: Methodology and writing—original draft preparation, C.D. and H.Y.; software and writing—review and editing, J.G., H.Y., L.C. and Z.F. All authors have read and agreed to the published version of the manuscript.

Funding: This work was funded in part by the Natural Science Foundation on Frontier Leading Technology Basic Research Project of Jiangsu under Grant BK20212001; in part by National Natural Science Foundation of China under Grants 62201052; in part by National Natural Science Foundation of China under Grant 62001029 and in part by Beijing Natural Science Foundation under Grant L202015.

Data Availability Statement: The data and code are available from the corresponding authors upon reasonable request.

Conflicts of Interest: The authors declare no conflict of interest.

Abbreviations

The following abbreviations are used in this manuscript:

IoT	Internet of Things
UAV	Unmanned Aerial Vehicle
BD	Backscatter Device
BackCom	Backscatter Communication
CE	Carrier Emitter
NOMA	Non-Orthogonal Multiple Access
SIC	Successive Interference Cancellation
BCD	Block Coordinate Descent
SCA	Successive Convex Approximation
LoS	Line-of-Sight
nLoS	Non-Line-of-Sight
SINR	Signal-to-Interference-plus-Noise Ratio
TDMA	Time-Division Multiple Access

References

1. Wang, K.; Qi, X.; Shu, L.; Deng, D.J.; Rodrigues, J.J. Toward trustworthy crowdsourcing in the social internet of things. *IEEE Wirel. Commun.* **2016**, *23*, 30–36. [CrossRef]
2. Etim, I.E.; Lota, J. Power control in cognitive radios, Internet-of Things (IoT) for factories and industrial automation. In Proceedings of the IECON 2016—42nd Annual Conference of the IEEE Industrial Electronics Society, Florence, Italy, 23–26 October 2016; pp. 4701–4705. [CrossRef]
3. Niu, Z.; Ma, W.; Wang, W.; Jiang, T. Spatial modulation-based ambient backscatter: Bringing energy self-sustainability to massive internet of everything in 6G. *China Commun.* **2020**, *17*, 52–65. [CrossRef]
4. Zhang, W.; Qin, Y.; Zhao, W.; Jia, M.; Liu, Q.; He, R.; Ai, B. A green paradigm for Internet of Things: Ambient backscatter communications. *China Commun.* **2019**, *16*, 109–119. [CrossRef]
5. Li, X.; Zheng, Y.; Khan, W.U.; Zeng, M.; Li, D.; Ragesh, G.K.; Li, L. Physical Layer Security of Cognitive Ambient Backscatter Communications for Green Internet-of-Things. *IEEE Trans. Green Commun. Netw.* **2021**, *5*, 1066–1076. [CrossRef]
6. Ye, N.; Yu, J.; Wang, A.; Zhang, R. Help from space: Grant-free massive access for satellite-based IoT in the 6G era. *Digit. Commun. Netw.* **2021**, *8*, 215–224. [CrossRef]
7. Darsena, D.; Gelli, G.; Verde, F. Modeling and Performance Analysis of Wireless Networks with Ambient Backscatter Devices. *IEEE Trans. Commun.* **2017**, *65*, 1797–1814. [CrossRef]
8. Liu, W.; Liang, Y.C.; Li, Y.; Vucetic, B. Backscatter Multiplicative Multiple-Access Systems: Fundamental Limits and Practical Design. *IEEE Trans. Wirel. Commun.* **2018**, *17*, 5713–5728. [CrossRef]
9. Kang, X.; Liang, Y.C.; Yang, J. Riding on the Primary: A New Spectrum Sharing Paradigm for Wireless-Powered IoT Devices. *IEEE Trans. Wirel. Commun.* **2018**, *17*, 6335–6347. [CrossRef]
10. Ouamri, M.A.; Singh, D.; Muthanna, M.A.; Bounceur, A.; Li, X. Performance analysis of UAV multiple antenna-assisted small cell network with clustered users. *Wirel. Netw.* **2023**, *early access*. [CrossRef]
11. Ouamri, M.A.; Alkanhel, R.; Gueguen, C.; Alohali, M.A.; Ghoneim, S.S.M. Modeling and Analysis of UAV-Assisted Mobile Network with Imperfect Beam Alignment. *Comput. Mater. Contin.* **2022**, *74*, 453–467. [CrossRef]

12. Ouamri, M.A.; Alkanhel, R.; Singh, D.; Sayed M. El-kenaway, E.; Ghoneim, S.S.M. Double deep q-network method for energy efficiency and throughput in a uav-assisted terrestrial network. *Comput. Syst. Sci. Eng.* **2023**, *46*, 73–92. [CrossRef]
13. Nguyen, T.H.; Park, H.; Park, L. Recent Studies on Deep Reinforcement Learning in RIS-UAV Communication Networks. In Proceedings of the 2023 International Conference on Artificial Intelligence in Information and Communication (ICAIIC), Bali, Indonesia, 20–23 February 2023; pp. 378–381. [CrossRef]
14. Truong, T.P.; Tuong, V.D.; Dao, N.N.; Cho, S. FlyReflect: Joint Flying IRS Trajectory and Phase Shift Design Using Deep Reinforcement Learning. *IEEE Internet Things J.* **2023**, *10*, 4605–4620. [CrossRef]
15. Yang, H.; Ye, Y.; Chu, X.; Sun, S. Energy Efficiency Maximization for UAV-Enabled Hybrid Backscatter-Harvest-Then-Transmit Communications. *IEEE Trans. Wirel. Commun.* **2022**, *21*, 2876–2891. [CrossRef]
16. Yao, C.; Liu, Y.; Wei, X.; Wang, G.; Gao, F. Backscatter technologies and the future of internet of things: Challenges and opportunities. *Intell. Converg. Netw.* **2020**, *1*, 170–180. [CrossRef]
17. Hua, M.; Swindlehurst, A.L.; Li, C.; Yang, L. UAV-Aided Backscatter Networks: Joint UAV Trajectory and Protocol Design. In Proceedings of the 2019 IEEE Global Communications Conference (GLOBECOM), Waikoloa, HI, USA, 9–13 December 2019; pp. 1–6. [CrossRef]
18. Tran, D.H.; Chatzinotas, S.; Ottersten, B. Throughput Maximization for Backscatter- and Cache-Assisted Wireless Powered UAV Technology. *IEEE Trans. Veh. Technol.* **2022**, *71*, 5187–5202. [CrossRef]
19. Yang, G.; Dai, R.; Liang, Y.C. Energy-Efficient UAV Backscatter Communication with Joint Trajectory Design and Resource Optimization. *IEEE Trans. Wirel. Commun.* **2021**, *20*, 926–941. [CrossRef]
20. Du, Y.; Chen, Z.; Hao, J.; Guo, Y. Joint Optimization of Trajectory and Communication in Multi-UAV Assisted Backscatter Communication Networks. *IEEE Access* **2022**, *10*, 40861–40871. [CrossRef]
21. Maraqa, O.; Rajasekaran, A.S.; Al-Ahmadi, S.; Yanikomeroglu, H.; Sait, S.M. A Survey of Rate-Optimal Power Domain NOMA With Enabling technologies of Future Wireless Networks. *IEEE Commun. Surv. Tutor.* **2020**, *22*, 2192–2235. [CrossRef]
22. Pan, J.; Ye, N.; Yu, H.; Hong, T.; Al-Rubaye, S.; Mumtaz, S.; Al-Dulaimi, A.; Chih-Lin, I. AI-Driven Blind Signature Classification for IoT Connectivity: A Deep Learning Approach. *IEEE Trans. Wirel. Commun.* **2022**, *21*, 6033–6047. [CrossRef]
23. Guo, J.; Zhou, X.; Durrani, S.; Yanikomeroglu, H. Design of Non-Orthogonal Multiple Access Enhanced Backscatter Communication. *IEEE Trans. Wirel. Commun.* **2018**, *17*, 6837–6852. [CrossRef]
24. Nazar, A.W.; Hassan, S.A.; Jung, H. BER Analysis of a NOMA Enhanced Backscatter Communication System. In Proceedings of the GLOBECOM 2020—2020 IEEE Global Communications Conference, Taipei, Taiwan, 7–11 December 2020; pp. 1–6. [CrossRef]
25. Ding, Z.; Poor, H.V. On the Application of BAC-NOMA to 6G umMTC. *IEEE Commun. Lett.* **2021**, *25*, 2678–2682. [CrossRef]
26. Ding, Z.; Poor, H.V. Advantages of NOMA for Multi-User BackCom Networks. *IEEE Commun. Lett.* **2021**, *25*, 3408–3412. [CrossRef]
27. Liu, Q.; Sun, S.; Hou, J.; Jia, H.; Kadoch, M. Resource Allocation in NOMA-Assisted Ambient Backscatter Communication System. *Electronics* **2021**, *10*, 3061. [CrossRef]
28. Tseng, P. Convergence of a Block Coordinate Descent Method for Nondifferentiable Minimization. *J. Optim. Theory Appl.* **2001**, *109*, 475–494. [CrossRef]
29. Bai, L.; Chen, Q.; Bai, T.; Wang, J. UAV-Enabled Secure Multiuser Backscatter Communications with Planar Array. *IEEE J. Sel. Areas Commun.* **2022**, *40*, 2946–2961. [CrossRef]
30. Hu, J.; Cai, X.; Yang, K. Joint Trajectory and Scheduling Design for UAV Aided Secure Backscatter Communications. *IEEE Wirel. Commun. Lett.* **2020**, *9*, 2168–2172. [CrossRef]
31. Hua, M.; Yang, L.; Li, C.; Wu, Q.; Swindlehurst, A.L. Throughput Maximization for UAV-Aided Backscatter Communication Networks. *IEEE Trans. Commun.* **2020**, *68*, 1254–1270. [CrossRef]
32. Wu, Q.; Zeng, Y.; Zhang, R. Joint Trajectory and Communication Design for Multi-UAV Enabled Wireless Networks. *IEEE Trans. Wirel. Commun.* **2018**, *17*, 2109–2121. [CrossRef]
33. Zeng, S.; Zhang, H.; Di, B.; Song, L. Trajectory Optimization and Resource Allocation for OFDMA UAV Relay Networks. *IEEE Trans. Wirel. Commun.* **2021**, *20*, 6634–6647. [CrossRef]
34. Dai, C.Q.; Li, S.; Wu, J.; Chen, Q. Distributed User Association with Grouping in Satellite—Terrestrial Integrated Networks. *IEEE Internet Things J.* **2022**, *9*, 10244–10256. [CrossRef]
35. Ben-Tal, A.; Nemirovski, A. *Lectures on Modern Convex Optimization—Analysis, Algorithms, and Engineering Applications*; MPS-SIAM Series on Optimization; SIAM: Philadelphia, PA, USA, 2001.